Integration of Gold Nanoparticles to Modulate the Ignitability of Nanothermite Films

Baptiste Julien, Jérémy Cure, Ludovic Salvagnac, Claudie Josse, Alain Estève, Carole Rossi

Integration of Gold Nanoparticles to Modulate the Ignitability of Nanothermite Films

*Baptiste Julien[1], Jeremy Cure[1], Ludovic Salvagnac[1], Claudie Josse[2], Alain Esteve[1], Carole Rossi[1,]**

[1]LAAS-CNRS, University of Toulouse, 7 Avenue du colonel Roche, 31077 Toulouse, France

[2]Centre de Microcaractérisation Raimond CASTAING, 3 rue Caroline Aigle, 31400 Toulouse, France

KEYWORDS: energetic materials, CuO, Al, STEM-EELS, Thermite multilayered films

Abstract:

Thermite multilayered films composed of alternating thin layers of metal/oxidizers have various uses in microelectromechanical systems (MEMS), microelectronics and materials bonding applications. Recently, applied research especially on the micro-initiator applications has engendered an urgent need to improve ignitability without changing the layering, reactant spacing that both affect the combustion characteristics. This work describes an innovative nano-engineering solution to reduce the energy barriers for mass transport making it possible to substantially lower ignition energy of CuO/Al reactive multilayers without manipulating the fuel and oxide layers thickness. To that end, gold nanoparticles exhibiting high thermal diffusivity properties are *in-situ* grown uniformly inside the first CuO layer to produce localized hot-spots

and promote the Al+CuO reaction. The CuO/Al reactive films with embedded gold nanoparticles exhibit earlier and optimized reaction than standard ones. The effect of gold nanoparticles on the thermite ignition mechanisms and the detailed reaction pathways were characterized by a host of characterization techniques including microscopy, thermal analysis, spectroscopy and X-ray diffractometric. Altogether, results show that the gold nanoparticles are seeding nodular defects with conical shapes provoking – under thermal stimulation- high stressed zones in the multilayer where the Al+CuO reaction is quickly triggered. The analysis of reaction products showed that the multilayers break the unreacted Al droplets early allowing them to burn into the environment. The results provide a behavioral baseline for future studies of interface engineering to tune internal stress-induced reaction in reactive thin films at large.

Introduction

Nanothermites have received increasing interest over the last two decades for additives in propellants,[1,2] combustion synthesis of advanced materials[3–5] and on chips energetics.[6–10] Different nanothermite systems were produced by different approaches including ball-milling, vapor deposition technique to produce nanopowders mixtures,[2,11–15] core-shell structure and nanofoils.[18–22] Among them, fully-dense Al/CuO multilayer materials represent an interesting system for both its potential applications and fundamental science perspectives. The former has spanned various areas including tunable initiation of secondary explosives,[7,23,24] joining, brazing and sealing.[25] The latter has particularly aimed at taking advantage of the fact that these materials offer a unique setting for analysing phase and structure transformations under external stimulation to understand the physics and chemistry involved in reaction processes. It is now well-admitted that the energetic properties of Al/CuO multilayer films are mainly governed by the mass transport and diffusion distance between reactant layers influencing both the combustion properties and materials

ignitability and sensitivity.[26–28] Three ways were explored in the literature to tailor the thermite multilayers reaction onset and reaction rate release: i) changing the reactant spacing and stoichiometry to affect the reaction kinetics and enthalpy,[29] or ii) changing the reactant nature, which induces a modification of the final oxide, directly impacting the oxygen diffusion.[30] But it also modifies the reaction products (sub-oxides in condensed and gaseous phase); or iii) engineering the interfacial layer to produce a more or less porous barrier for the oxygen to diffuse through.[31–33]

In parallel, applied research on micro initiator based applications has engendered an urgent need to improve ignitability, i.e. moderate ignition energy of the thermite film (energy needed to trigger the Al+CuO reaction by Joule effect, i.e. thermal initiation), without changing the layering, reactant spacing and Al/CuO mass ratio in the multilayer, which all define the total energy release, and flame temperature.

In this respect, we propose to *in-situ* grow gold nanoparticles (GNP) exhibiting high thermal diffusivity properties (127.10^{-6} $m^2.s^{-1}$, i.e. well above the Al or CuO materials) inside the first CuO layer to produce localized hot-spots, and thus promote the redox reaction without adding an interfacial layer or manipulating the fuel and oxide layers thicknesses. CuO/Al films with embedded GNP (CuO/Al-GNP) exhibit earlier reaction than standard ones: the ignition energy is lowered by 82 % whereas the flame duration and intensity remains equal.

This study seeks to experimentally correlate observed ignition and reaction performances with local microstructure in CuO/Al-GNP multilayers using a host of characterization techniques including electronic microscopy, energy electron loss spectroscopy, thermal analysis and X-ray diffraction and identify if the GNP serves as localized heat absorbers to produce high stressed zones in the multilayer that could react under thermal stimulation.

Materials and Methods

Material preparation. As the Al/CuO multilayers system is well documented and characterized, it provides an ideal model-system to study the effect of mechanical properties on thermal initiation. Two Al rich CuO/Al multilayers (samples) were prepared. The first one consists of 15 bilayers of CuO/Al in which gold nanoparticles (GNP) are integrated into the first layer of CuO. The second composite is a reference sample consisting of 15 bilayers of CuO/Al. The two samples are named thereafter CuO/Al-GNP and CuO/Al-ref, respectively. The multilayer stacks are chosen to be consistent with previous works related to integration of CuO/Al nanolaminates in MEMS for ignition applications[6] : the Al/CuO bilayer thickness is set at 400 nm. The Al to CuO mass ratio is therefore 2:1 (fuel-rich configuration), i.e. Al and CuO thicknesses are 200 nm.

The multilayer stacks are magnetron-deposited following a procedure previously described.[26,34] In summary, Al and CuO are sputtered from Cu and Al targets (8 by 3 inches sides and ¼ inches thick) using a base pressure of 5.10^{-7} mbar. O_2 and Ar gases flow rates of 16 and 32 SCCM are used respectively for cupric oxide deposition with a partial pressure of 10^{-2} mbar. The Ar partial pressure during Al deposition is maintained at 5.10^{-3} mbar. The sample is cooled at ambient temperature for 600 s at the end of the deposition process.

Photo-deposition of Gold nanoparticles. The GNP photo-deposition process is adapted from a previously reported method.[35] A 100 nm thick CuO film, sputter-deposited on a SiP wafer or glass wafer, is immersed in a mixture composed by 50 mL of $HAuCl_4$ aqueous solution (precursor, $[Au^{3+}] = 2.5.10^{-4}$ mol.L^{-1}), 0.15 mL of sodium citrate aqueous solution ([citrate] = 0.05 mol.L^{-1}), 4.85 mL of deionized (DI) water and 5 mL of ethanol in order to have a final [citrate]/$[Au^{3+}]$ ratio value of 0.6. The immersed wafer is then UV irradiated during 10 min at the power of 100 W. The sample is then dried and annealed in air at 120 °C during 10 min to ensure the anchorage of GNP

in the CuO surface. After the annealing step, the samples are vigorously cleaned with DI water (around 75 mL for each sample) to remove all the by-products arising from the thermal decomposition of the citrate ligands. The presence of GNP is confirmed by grazed incidence X-ray diffraction (GI-XRD and TEM-EDS, see supporting information Figure S1).

Characterization. The CuO/Al multilayer films were first examined using a FEI Helios NanoLab DualBeam scanning electronic microscope (SEM). The images were obtained using a backscattered electron detector to achieve a good contrast. The elementary composition is estimated by energy dispersive X-ray analysis (EDX), with a JEOL CENTURIO-X SDD detector.

Transmission electronic microscope (TEM) cross-sectional lamellas were prepared using a focused-ion beam FIB-SEM FEI Helios NanoLab DualBeam. TEM lamellas were characterised by high-magnification TEM and scanning TEM (STEM) using a JEOL JEM-ARM200F cold-FEG instrument, operated at 200 kV. The maximum spatial resolution (in STEM mode) is 0.078 nm. The chemical composition was analysed by energy electron loss spectroscopy (EELS), using a GIF Quantum ER imaging filter.

The phase composition of the prepared multilayers was determined using GI-XRD. This was done using a Bruker D8 Discover system with a Cu Kα radiation source, λ = 1.5418 Å. The measurements were performed in 2θ mode, from 20° to 80°, with a step of 0.02°. Further characterization of the multilayers is done through differential scanning calorimetry (DSC) using a NETZSCH DSC 404 F3 Pegasus device. The device is equipped with a DSC-Cp sensor type S and a Platinum furnace in a temperature range from room temperature to 1000 °C. Thermal analyses were performed under constant heating rates (10 - 40 °C/min) in Ar atmosphere (99.998% pure) at a flow rate of 20 mL.min^{-1}. The traces were normalized by the mass of nanothermite material (around 5 mg).

By varying the heating rates, activation energies for each reaction peak were determined using the peak temperature (T_p) fits to the Kissinger kinetic model using eq. (1).

$$\ln\left(\frac{\beta}{T_p^2}\right) = \ln\left(\frac{AR}{E_a}\right) - \frac{E_a}{RT_p} \qquad \text{(Eq. 1)}$$

where E_a is the activation energy, $\beta = dT/dt$ is the heating rate, T_p is the peak temperature, R is the gas constant and A is the pre-exponential factor. By plotting $\ln(\beta/{T_p}^2)$ versus $1/T_p$ (Kissinger plot), one can easily extract E_a by calculating the slope for each reaction peaks.

The stress magnitude is determined using a KLA-TENCOR P17 stylus profiler, by measuring the change in the substrate curvature before and after the film deposition. The residual stress σ is inversely proportional to the change curvature radius, following the Stoney equation (eq. 2)[36]:

$$\sigma = \frac{E_s}{6(1-\nu_s)}\frac{h_s^2}{h_f}\left(\frac{1}{R} - \frac{1}{R_0}\right) \qquad \text{(Eq. 2)}$$

with E_s the Young modulus of the substrate, ν_s the Poisson's ratio of the substrate, h_s the substrate thickness, h_f the film thickness, R_0 and R the curvature radii of the substrate before and after the film deposition.

Ignition experiments. The sustained reactions in CuO/Al multilayer films can be initiated via a localized hot point such as a resistive filament, resulting in self-propagating combustion fronts that propagate away from the ignition source. On-chip resistive filament (See Supporting Information Figure S2) was fabricated as follows: a 500-µm thick 4-inch glass substrate is cleaned with an oxygen plasma at 800 W for 5 min to remove surface contaminations. Next, 800-nm thick titanium and 300-nm thick gold layers are evaporated onto the surface and then patterned to define the Ti filament and Au electrical pads.

The electrical resistance obtained is 3 ± 0.2 Ω. Finally, around 12 mm² CuO/Al multilayer films are patterned and sputter-deposited, as described previously in contact with the Ti filament. At the end the chip is 6.7 × 5.6 mm.

The Ti thin film filament is heated using a dc current of 1.8 ± 0.1 A (with a compliance of 20 V) corresponding to a dissipated electrical power of 10 W. This value is reached accounting for a residual resistance value (0.7 ± 0.1 Ω) of the electrical setup. This corresponds to a heating rate of 10^5-10^6 K.s^{-1}, estimated by a numerical Joule heating model, detailed in Supporting Information S3. The ignition delay of the multilayers is characterized using a photodiode (VISHAY, reference BPV10) polarized at 5 V placed at a few inches distance from the thermite, capable to detect and record the optical emission. The current emitted by the photodiode illuminated by the thermite reaction is measured through a dummy resistance of 1 kΩ. All the data were processed using a homemade MATLAB code. A visual of the experimental setup is presented in Supporting Information, Figure S2.b. For each type of sample, the measurements were repeated 10 times, and the statistical values are reported.

Results and discussion

Samples characterization

High magnification TEM and SEM micrographs of CuO/Al-GNP are shown in Figure 1, revealing the GNP distribution and the internal structure of the first CuO layer. The images are taken in dark field, so the lightest elements appear in dark (Al) whereas the heaviest appear in bright (Au, CuO). GNP is distinguished by its high brightness (Figure 1b) inside the first CuO layer. The GNP size is 5-20 nm wide and its size dispersity is reported in Figure 1c. The size distribution was obtained by taking several SEM pictures at different magnification of the CuO surface. For each image, the particles were counted using ImageJ analysis software. A minority of

bigger particles probably made of gold clusters, of a few hundreds of nanometers across are also observed. The EDS mapping (not shown) supports the presence of the different elements in each layer. The Al and CuO layers exhibit overall structures that are typical of conventional CuO/Al films, i.e. columnar CuO and polycrystalline Al layers. However, in contrast to the reference sample, CuO/Al-GNP exhibits a few defects that develops from the bigger GNP seeds (~ 100 nm in diameter) as conical shaped defects, resulting in the formation of spherical bumps at the surface of the nanolaminate. These defects and their evolution will be described in more details in subsection *Structure morphology evolution upon heating*. The XRD patterns for all multilayers specimens are presented in Supporting Information S4. Al and CuO are clearly detected whereas crystalline Au is not observed, probably due to the deep localization of the GNP within the film having a total thickness of 6 µm.

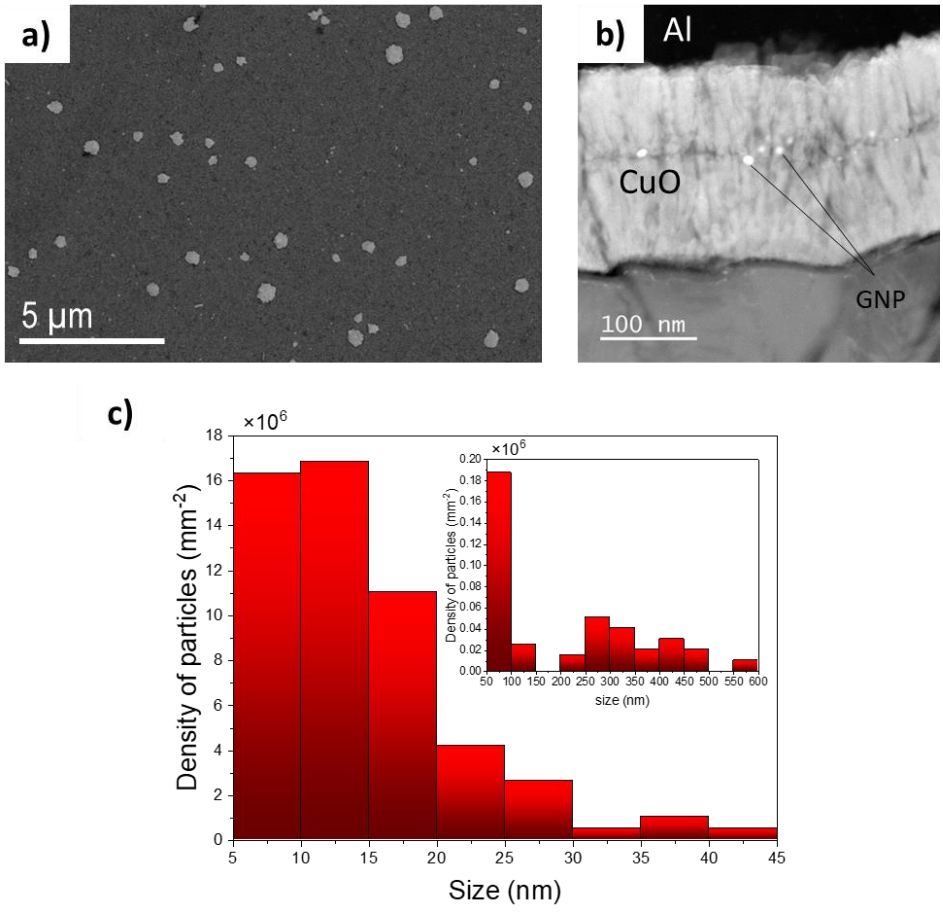

Figure 1*. a) SEM image of GNP deposited on a 100 nm-thick CuO layer; b) TEM image of the CuO/Al/GNP cross section and; c) size distribution of gold particles (GNP).*

Ignition experiment.

For each sample (CuO/Al-GNP and CuO/Al-ref), the measured ignition delay under 10 W electrical input and flame characteristics are shown in Figure 2 and summarized in Table 1.

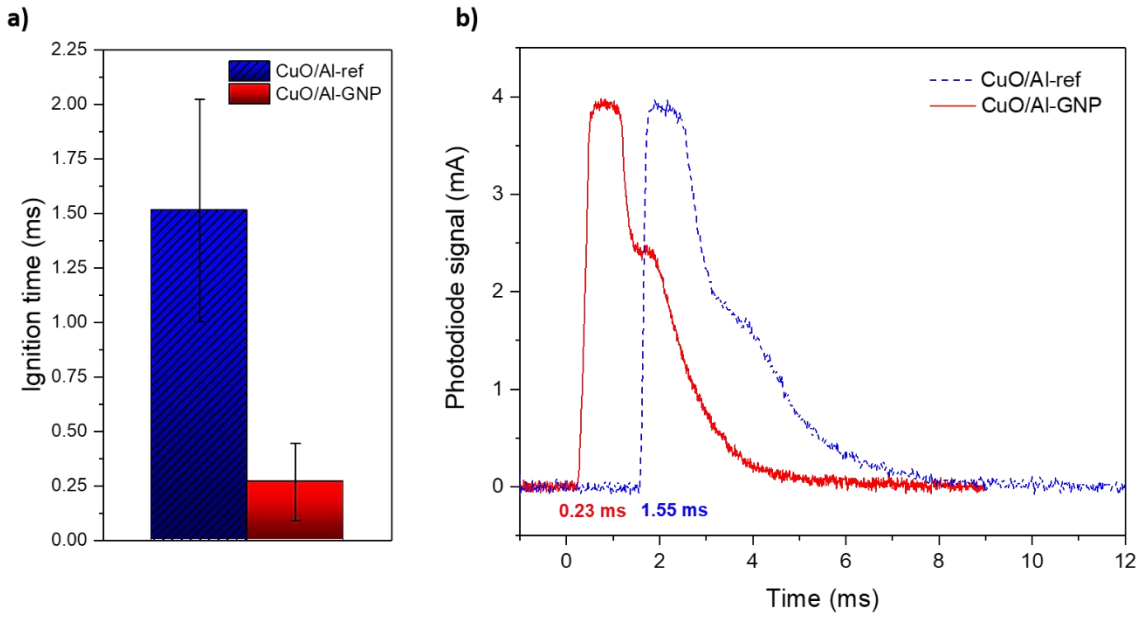

Figure 2*. Result of ignition experiments for CuO/Al-ref and CuO/Al-GNP: a) ignition delay and; b) an example of photodiode signals acquired during ignition.*

A clear difference in the ignition delay is observed between the two samples in Figure 2. Samples with GNP are ignited almost 6 times faster than reference ones: 0.3 ms for CuO/Al-GNP versus 1.5 ms for the reference (Figure 2a). The standard deviation of the ignition delay is about 0.2 ms for CuO/Al-GNP and 0.5 ms for the reference (see errors bars of the graph in Figure 2a). Finally,

the analysis of the photodiode signals (one example is shown in Figure 2b) gives us some information about the energy properties, i.e. flame intensity and duration. The maximum intensity of the photocurrent and the signal width can be respectively related to the maximum temperature and the duration of the flame produced by the nanothermite combustion. The integral of the photodiode signal provides information regarding the total energy liberated during the combustion. Those characteristics are well preserved when GNP are integrated into the thermite: the flame intensity is the same (maximum photodiode current of 3.9 mA for both samples), whereas the signal width and integral are slightly shorter: the signal widths are 7 ± 1 and 8 ± 1 ms and the integral of the photodiodes are 7.9 and 8.7 a.u. for CuO/Al-GNP and CuO/Al-ref, respectively (Table 1).

Table 1. *Results of ignition experiments (mean value calculated on 10 ignition experiments for each sample).*

		Photodiode signals characteristics		
	t_{ignit} (ms)	Maximum (mA)	Width (ms)	Integral (a.u.)
CuO/Al-ref	1.5 ± 0.5	3.95 ± 0.10	8 ± 1	8.7 ± 0.5
CuO/Al-GNP	0.3 ± 0.2	3.89 ± 0.04	7 ± 1	7.9 ± 0.5

Thermal analysis.

DSC analysis is routinely used to characterize energetic materials and provides details about exothermic events and total amount of energy released from materials. Figure 3 shows the DSC traces obtained for the different samples heated from the ambient to 1000 °C at a heating rate of

20 °C.min^{-1} under a controlled flow of Argon (See Supporting Information S5 for DSC repeatability).

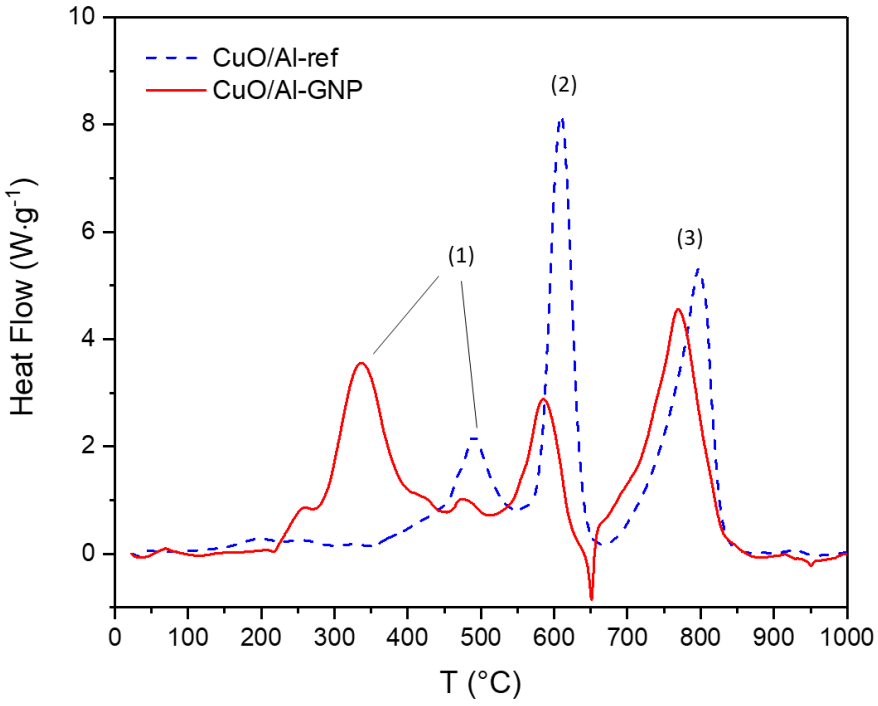

***Figure 3**. DSC traces of foils composed of 15 bilayers of CuO/Al-ref (blue dash curve) and CuO/Al-GNP (red solid curve), collected at 20 °C.min^{-1}.*

The DSC trace obtained for reference multilayers (blue dash curve of Figure 3) is very similar to traces already published in the literature for fuel rich configuration.[26] We observe three exothermic events. A first broad exothermal (1) event is observed between 350 and 550 °C with a peak temperature at 490 °C. It is followed by a strong exothermal peak at 550 - 650 °C with a peak temperature at 609 °C. A last exotherm at high temperature is detected between 700 and 840 °C, with a peak at 797 °C. Around 250-300 °C the copper oxide releases oxygen atoms[37,38] that diffuse across the natural interfacial layers to oxidize the neighbouring aluminium, thus forming amorphous alumina. Because amorphous alumina density is substantially higher than that of the naturally grown interface, its structure is mechanically degraded at ~350 °C leading to the

accelerated redox reaction.[39] Then, the resulting increase in amorphous alumina layer thickness provides a barrier to the oxygen diffusion that slows down Al oxidation, thus reducing the heat release corresponding to the drop of the first exotherm in the DSC trace (1). The second exothermal peak (2) corresponds to the main reaction stopped by a polymorphic phase change (amorphous alumina → γ-Al_2O_3). Then Al oxidation, in liquid phase, continues through the γ-Al_2O_3 (3), which process is activated at 700 °C.

The thermal analysis of CuO/Al-GNP (red solid curve of Figure 3) reveals a much more complex behavior with a wider temperature profile, showing substantial differences in the two first exotherms (200-600 °C regime) while exhibiting similar exothermic behaviours in the higher temperature regime. Importantly, reaction onset is dramatically shifted down to ~ 200 °C (350 °C for the reference). This first exotherm peak temperature is located at 337 °C instead of 490 °C for the reference sample and is composed of multiple elementary contributions. The second peak (2) is a bit shifted down to 586 °C and features an intensity almost 3 times lower than that of the reference. It appears that the first reaction step (oxidation of neighbouring aluminium to form amorphous alumina) is enhanced when the GNP are integrated into the first CuO layer. This is further discussed in sub-section *Structure morphology evolution upon heating* showing the evolution of the multilayer structure upon heating. Note that we also notice a bump at ~ 475 °C, exactly centred on the first exotherm of reference sample, which could be associated to Al oxidation in the multilayer far from the GNP.

The heats of reaction for each peak, calculated by integrating the DSC curves over the time in the different temperature ranges, are reported in Table 2.

Table 2. *Enthalpy of reaction calculated by integrating the exothermic signal over time and normalized with respect to the film mass.*

	Theoretical ΔH (J/g)[18]	Total ΔH (J/g)	**Heat of reaction per peak (J.g^{-1})**		
			Exotherm (1)	Exotherm (2)	Exotherm (3)
CuO/Al-ref	3300	2651	561	1012	1078
CuO/Al-GNP		2986	1269	554	1163

The experimental ΔH of CuO/Al-ref is only 80% of the theoretical value. Thus, only 80% of the aluminium available in the layers reacts. This is mainly due to parasitic reactions, such as the formation of Al-Cu intermetallic which occurs before 500 °C[38] and therefore consumes a portion of the reservoir as the Al-Cu bond formation is much less energetic than that of Al-O bond.

Compared to CuO/Al-ref, the CuO/Al-GNP multilayers feature a total experimental ΔH closer to the theoretical value (90%), which means that the Al reservoir is more efficiently and quickly consumed. In CuO/Al-GNP sample, more than double mass of Al reacts with oxygen during the first exotherm. Consequently, the second exotherm (2) is less intense. This can be explained by two main reasons: (i) the CuO/Al-GNP features much more interfacial area due to the presence of conical nodules, (ii) also, the high-stress magnitude at the cones' boundaries lowers the diffusion barrier of O through interfacial layer. As a result, as soon as the CuO releases its oxygen (~250-300 °C), neighbouring aluminium quickly oxidizes. The amorphous alumina formed by this solid-state reaction produces a barrier that causes the end of the first peak as it is the case in CuO/Al-

ref. Then the oxidation is again activated (second peak (2)) when the diffusion of oxygen through amorphous alumina is thermally activated. Finally, the third reaction step, corresponding to the oxidation of melted Al (peak (3)) occurs and produces equivalent energy in both sample configurations, as expected since GNP only modify the first reaction step.

Next, we applied the Kissinger's method which is intensively used in interpreting DSC data for thermite materials, in order to calculate activation energies (E_a) for each reaction step (and for each sample). The concept of reaction progress on which is based the Kissinger method, should be limited to independent reactions occurring successively after each other, within specific temperature ranges, which is not the case in our thermite system where elementary physical mechanisms interact with each other and occur concurrently at all temperatures, therefore the determination of E_a is made with inaccuracies.

The activation energy (Figure 4) of the first exotherm (1) is highly reduced (by 61 %) by the presence of GNP, whereas the activation barriers of second and third exotherms are less affected by the GNP: E_a is only lowered by 18 % and 13 % for the second and third exotherms, respectively. For each sample, three DSC traces were considered and very reproducible. The numerical error on the linear fit for the first peak is about ±12 kJ.mol^{-1}the DSC.

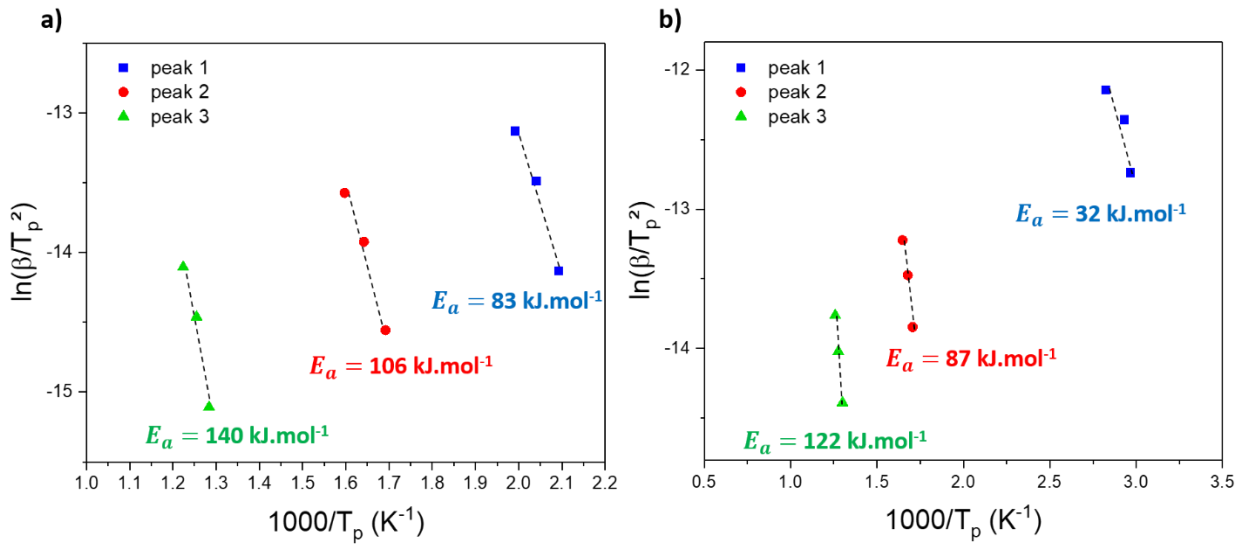

Figure 4*. Kissinger plots of a) CuO/Al-ref and b) CuO/Al-GNP, giving the activation energies (E_a) for the three reaction steps.*

As summary, the thermal analyses showed that the Al+CuO redox reaction starts at lower temperature, highly promoted when GNP are integrated in the first CuO layer. In order to understand the role of GNP in the Al+CuO reaction mechanisms, the structural and chemical changes of the CuO/Al-GNP sample were observed by HR-TEM, EELS in STEM mode upon annealing at 400 °C @ 10 °C/min.

Structure morphology evolution upon heating.

Figure 5 shows cross-sectional images of CuO/Al-GNP samples, as deposited (Figure 5a) and after *ex situ* annealing at 400 °C in argon atmosphere (Figure 5b). HR-TEM micrographs of reference (Figure 5c,d) and CuO/Al-GNP (Figure 5e,f) are also presented, with zooms on the microstructure. The large bright spot located in the first CuO layer (Figure 5a) is a zoom on one gold particle being ~100-200 nm in size. We clearly see that, the presence of the GNP alters the layers shape, and forms "nodular defects". The nodules form parabolic shapes, from the gold seeds

of diameter d to the dome surface of diameter D (Figure 6), following the relation: $D^2 \sim T \times d$, with T the Al/CuO multilayered film thickness.

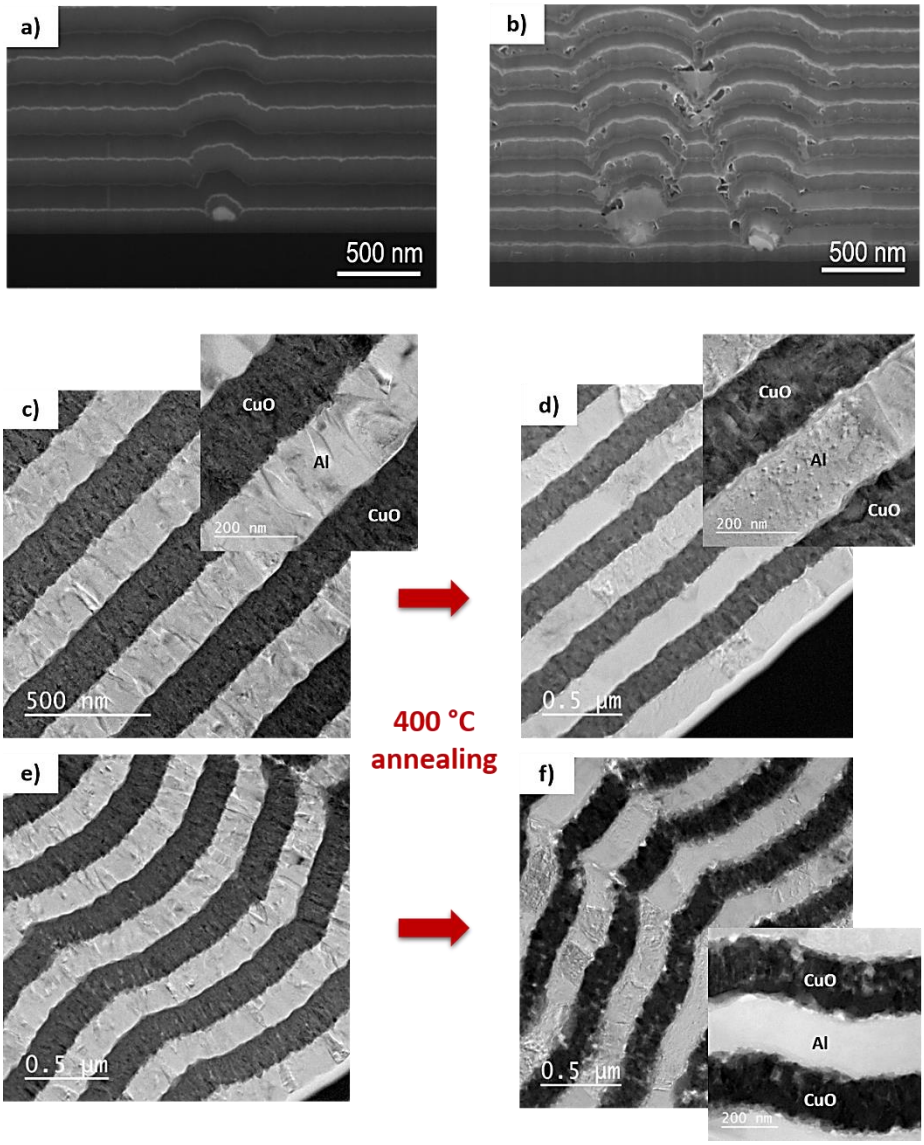

Figure 5. *Cross-sectional images of a) one as-deposited CuO/Al-GNP and b) 400 °C annealed CuO/Al-GNP. HR-TEM micrographs of c) as–deposited CuO/Al-ref; d) 400 °C annealed CuO/Al-ref; e) as–deposited CuO/Al-GNP and f) 400 °C annealed CuO/Al-GNP.*

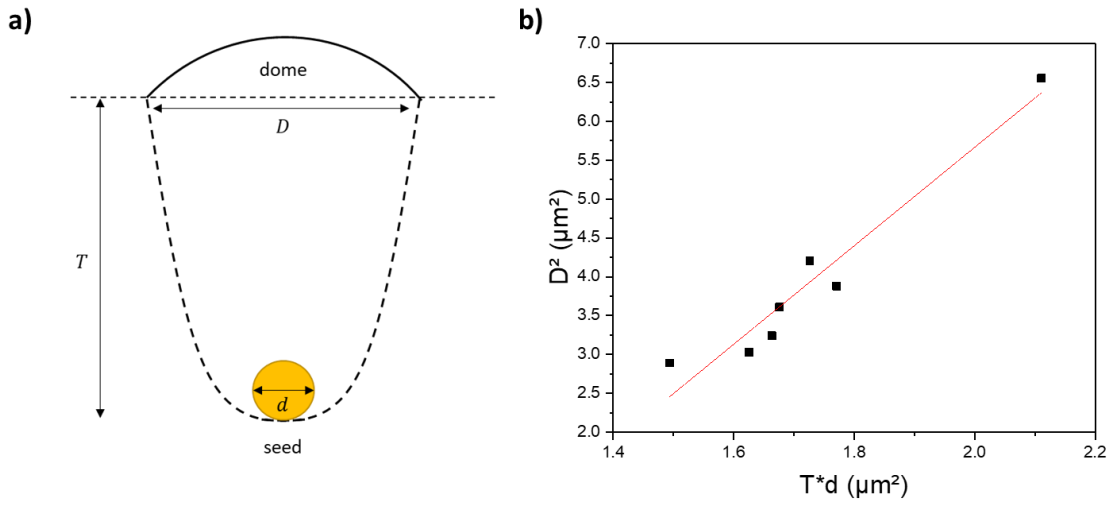

Figure 6*. Geometrical characterization of nodular defects presenting a) a schematic of a nodule induced by a particle (seed) with a diameter d and b) experimental relation between d and D parameters.*

The film stress magnitude with and without GNP evaluated by *ex situ* wafer-curvature measurements after multilayer growth is 240 MPa and 319 MPa for CuO/Al-GNP and CuO/Al-ref, respectively, clearly pointing that the GNPs integrated into the first CuO layer do not weaken the film, but rather relax the stress through local deformation (nodular defects).

After ramping up to 400 °C, we observe an important structural damage (Figure 5b) and morphological changes. The damage is also observed in TEM (Figure 5f). Numerous cracks, holes and voids appear as well as alumina portions. While most of these defects are clearly decorating the nodule boundaries, some are also dispersed in the multilayers, at the reactant interfaces. As a consequence, the reactant interfaces are now ill-defined with thicknesses varying from 20 to 50 nm, which represents about 10 to 25 % of the Al layer. Furthermore, the initial columnar structure of the CuO grains is partially lost after the annealing step, which testifies the densification of oxide

layers after its reduction (see EELS section). To summarize, we believe that damage of the multilayer locally favors the contact between the Al and CuO reservoirs through highly defective interfaces, which in turn will favor the diffusion of oxygen atoms from CuO to Al layers. Note that these damages, or extended defects, are also consistent with the enhancement of the first DSC peak as compared to the reference (Figure 3). Interestingly, Dong *et al.*[40] showed that mechanical stress affects the diffusivity of oxygen atoms by reducing the activation energy barrier for their migration through the interfacial layer, leading to an enhancement of the oxidation rate (the alumina growth being diffusion limited, as the oxidation reaction of aluminium is spontaneous).

For comparison, CuO/Al-ref has been observed after being annealed in the same conditions (Figure 5c and Figure 5d). Without GNP, the multilayers structure remains intact and we observe a substantial thickening of the interfacial alumina from 4 nm to about 15 nm without formation of extended defective domains as observed with GNP, which is in good agreement with the previous observations.[38]

Chemical evolution upon heating.

Additionally, crystalline phases are examined by GI-XRD. Typically, in the deposited films, only Al and CuO phases are detected. After annealing at 400 °C, the CuO is partially reduced into Cu_2O. The XRD spectra (Supporting Information S6) show a clear increase and well-defined Cu_2O peaks with a small detection of a broad Cu peak for the CuO/Al-GNP sample. A crystalline Al_2O_3 phase is not yet detected, as it is still in its amorphous phase.

Electron Energy Loss Spectroscopy carried out in scanning mode was used to correlate elemental distribution of atoms (namely Cu and Al atoms) with structural aspects derived from both TEM images and XRD spectra (CuO, Al, interfaces and their phases changes), after annealing at 400

°C. The Figure 7a and Figure 7b show high magnification TEM images and EELS diagrams taken in two different high-stressed zones around one nodule's boundary (represented in black dash line). Following the contrast, the oxide layer appears in bright while Al is dark. The Energy Loss Near Edge Structure (ELNES) is acquired along lines scan of 130.5 nm and 285.6 nm, with a step of 14.5 and 23.8 nm respectively (indicated by the colour bar on the micrographs). The first diagram (Figure 7a) is acquired along the non-well defined interface between oxide and Al layers, while the second one (Figure 7b) is taken inside a failure at the nodule boundary. The Cu-L-edge ELNES is characterized by two main peaks corresponding to the transitions of $2p_{1/2}$ (L_2) and $2p_{3/2}$ (L_3) electrons toward 3d orbitals, around 933 and 955 eV respectively. The L_2 peak intensity represents roughly the half of the L_3 intensity, which is consistent with previous work.[41,42] The O-K-edge ELNES, is characterized by a weak peak at around 532 eV. Note that the background intensity of spectra is always subtracted using a power law fit. The complete EELS diagrams can be found in Supporting Information S6.

By getting closer to the Al layer (from black to red in the line scan of Figure 7a the Cu-L_3 peaks are shifted to higher energies (932.7 eV to 935.1 eV), which corresponds to the reduction from Cu^{2+} to Cu^{+} ($4\ CuO \rightarrow 2\ Cu_2O + O_2$). A similar shift appears for L_2 edge. Moreover, we can notice that the first three L_3 peaks (in black) are not sharp peaks and exhibit a second maximum, which matches with Cu^{+} peaks at 935.1 eV (in orange). Thus, the bright layer would not be just CuO, but composed by co-existing CuO and Cu_2O phases. It is also possible that other metastable phases, such as Cu_4O_3 coexist too, which is difficult to assess from our data. This shows that, at 400 °C the reduction process is already in an advanced stage, in particular around critical zones where mechanical fractures are developed, which is in good agreement with the previous DSC analysis (Figure 3).

Concerning the Figure 7b, the line scan peak at 532 eV in the O-K edge ELNES indicates the presence of portions of alumina following the nodule boundary and positioned within the Al layer. Such a defect and its location are never observed in conventional Al/CuO stacks, where alumina is always located at the Al/CuO interface.[38] Interestingly, we notice a pre-peak around 524 eV which is consistent with the presence of gaseous oxygen (similar to oxygen molecules signature), liberated during the reduction of CuO ($4\ CuO \rightarrow 2\ Cu_2O + O_2$), which has already been observed in previous works.[43] The presence of gaseous oxygen and defects could possibly enhance the degradation and mechanical failure of the multilayers along the boundary, by facilitating oxygen migration pathways towards Al layers whereas in conventional Al/CuO multilayers, the O release and subsequent alumina growth occurs only at the interface.[38]

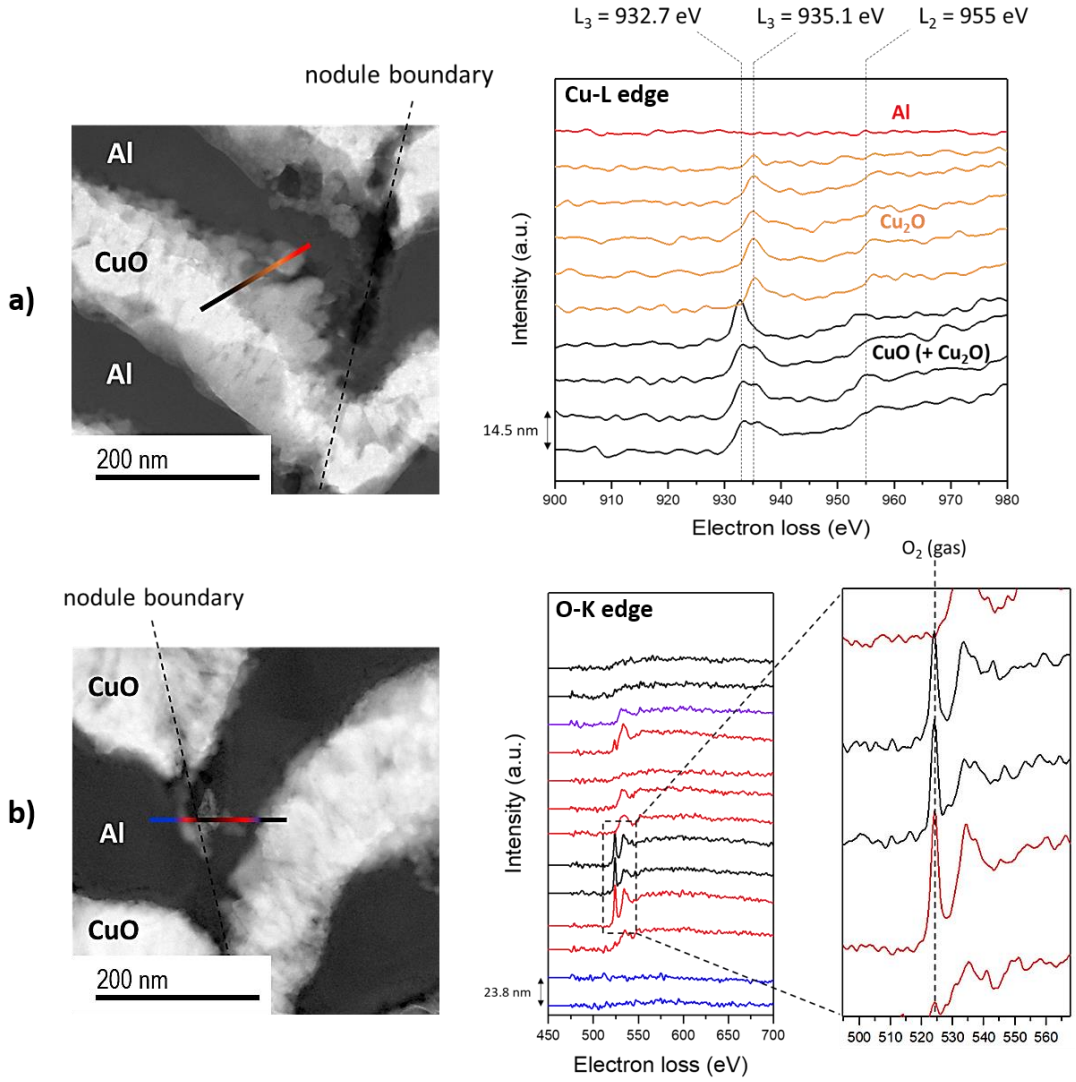

Figure 7*. EELS spectra of a) Cu-L edge and b) O-K edge acquired within CuO/Al-GNP sample, along a line scan (black dashed line) displayed on the corresponding TEM micrograph on the left. The background intensity of spectra is always subtracted using a power law fit.*

Reaction leading to ignition.

The mechanisms described in previous sections make it possible to interpret the ignition results and DSC analysis obtained for CuO/Al-GNP samples in comparison with CuO/Al-ref. Integrating GNP inside the reactive film induces nodular defects around nanoparticles, especially around the largest gold aggregates whose size is in the order of one hundred of nanometers, alters the shape

of layers along parabolic boundaries. At room temperature, the CuO/Al-GNP films are thermally stable and do not exhibit any increase of the mechanical stress compared to the reference. However, under thermal stimulation, the Al+CuO reaction quickly initiates, preferentially in the nodular defects, and at the seeding location surrounding nanoparticles.

As gold features a high thermal diffusivity (127.10^{-6} $m^2.s^{-1}$), much higher than CuO (9.10^{-6} $m^2.s^{-1}$), we suggest that the GNP absorbs heat, and, locally and quickly reaches high temperature thus producing high thermal stress. The stress propagates along the conical boundaries induced by GNPs, as observed by TEM images, unravelling chemical reactions and defect extension along these boundaries and across the layers. Then, when the local stress magnitude reaches a critical value, difficult to estimate or measure, the multilayer film disintegrates and pieces of unreacted Al are ejected and burn in condensed as gas phase in the surrounding environment as supported by the analysis of the reaction debris.

Microscopy images of reaction debris (Figure 8) that have been collected after the reaction show that both CuO/Al-ref and CuO/Al-GNP produce two types of residues: micron-sized spherical particles of alumina (2-5 µm in diameter) mixed with some larger (10-50 µm in size, not shown in the images) random shaped aggregates made of two components: alumina and copper (See Supporting Information Figure S8 for chemical mapping). Importantly, CuO/Al-GNP samples produce much more debris than CuO/Al-ref ones: 1289 residues / mm^2 for CuO/Al-GNP samples versus 227 residues / mm^2 for CuO/Al-ref. Debris analysis clearly supports that most of the reactional process proceeds in the condensed and gas phase in the air.

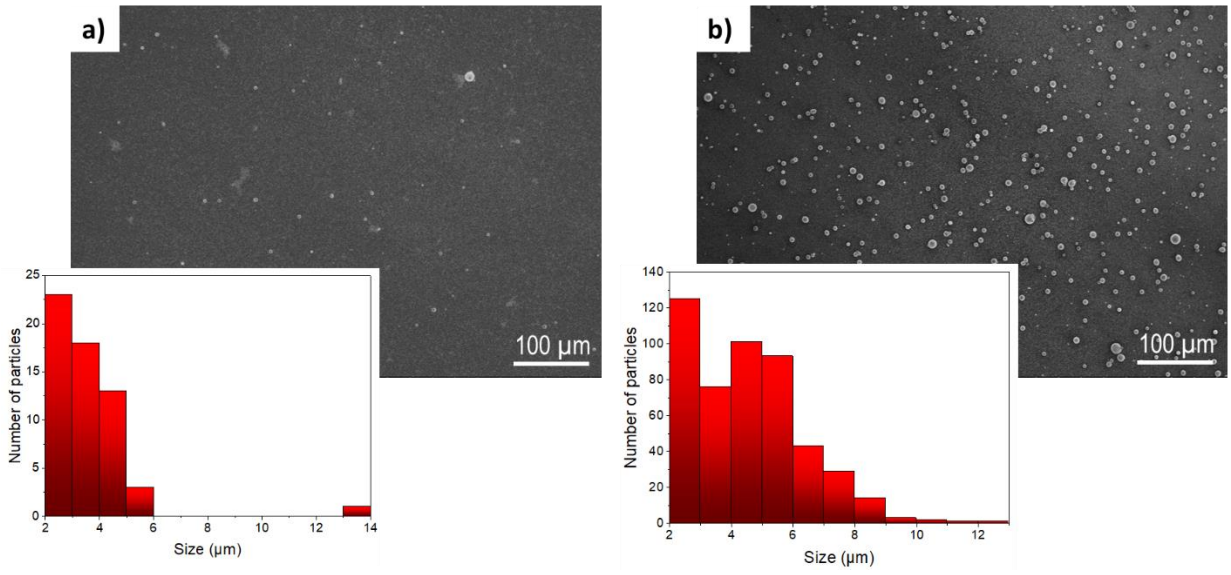

***Figure 8**. SEM images of reaction residues from the Al+CuO reaction, for a) CuO/Al-ref and b) CuO/Al-GNP collected on Si wafers during the ignition experiments. Inset histograms show the sizes distribution of residues.*

Conclusion

In this work, we have proposed an innovative nano-engineering solution to reduce the energy barriers and consequently the ignition temperature of CuO/Al reactive multilayers without manipulating the fuel and oxide layer thickness. Gold nanoparticles (5- 25 nm in size with some being 100 nm in size) are uniformly grown inside the first CuO layer. At room temperature, the CuO/Al films with gold nanoparticles inside are mechanically and thermally stable. But, under thermal stimulation, the Al+CuO reaction triggers at low temperature, 250 °C against 400 °C for same thermite films without nanoparticles. This leads to faster ignition delays, being roughly one third of those obtained for reference thermite films without nanoparticles. From microscopic observations, we deduced that gold nanoparticles embedded into the CuO matrix serve as localized heat absorbers. Under thermal stimulation, they produce localized hot-spots and thus induce

highly–stressed zones that trigger the Al+CuO reaction at 250 °C whereas standard CuO/Al films initiate at 400 °C. We also experimentally showed that the CuO/Al films with embedded gold nanoparticles exhibit more efficient reaction compared to standard ones: the heat of reaction reaches 90 % of the theoretical value against ~80 % for standard multilayered films. Finally, the analysis of reaction products showed that the multilayer early breaks projecting unreacted Al droplets that burn into the environment. We consider that these results open new perspectives in the field of interface engineering. While the leading trend was focused on the chemical modification of barrier layers or thicknesses/reactant ratio, we here propose a more versatile and efficient way to tune the thermite reaction by controlling its internal stress.

Associated content

Supporting Information

Details on the ignition device and experimental setup for ignition tests; the thermal model used to predict ignition temperature; XRD and TEM-EELS characterizations of the Al/CuO-GNP as deposited and after annealing at 400 °C; SEM-EDS images of reaction debris; DSC curves of Al/CuO-GNP foils. This material is available free of charge via the Internet at http://pubs.acs.org.

Author information

Corresponding author

Correspondence to: Carole Rossi, carole.rossi@laas.fr

Author contributions

B. J. prepared the samples and performed all the characterization measurements. J. C. performed the gold nanoparticles deposition and stabilization. C. J. prepared the lamellas and performed the microscopic observations. A. E. provided support the manuscript preparation. C. R.

provided support for the manuscript preparation and supervised the research. The manuscript was written through contributions of all authors. All authors have given approval to the final version of the manuscript.

Competing financial interests

The authors declare no competing financial interests.

Funding Sources

C.R. received funding from the European Research Council (ERC) under the European Union's Horizon 2020 research and innovation programme (grant agreement No 832889 - PyroSafe). L.S. received funding for sputter deposition equipment from FEDER/Region Occitanie program Grant THERMIE.

Acknowledgment

The authors acknowledge support from the European Research Council (H2020 Excellent Science) Researcher Award (grant 832889 – PyroSafe) and the Occitanie Region / European Union for their FEDER support (THERMIE grant). The authors thank Séverine Vivies from LAAS-CNRS and Teresa Hungria-Hernandez from “Centre de Micro Caractérisation Raymond Castaing (UMS 3623)” for their great support with samples preparation and TEM experiments.

References

(1) Prakash, A.; McCormick, A. V.; Zachariah, M. R. Tuning the Reactivity of Energetic Nanoparticles by Creation of a Core−Shell Nanostructure. *Nano Lett.* **2005**, *5* (7), 1357–1360. https://doi.org/10.1021/nl0506251.

(2) Dreizin, E. L. Metal-Based Reactive Nanomaterials. *Progress in Energy and Combustion Science* **2009**, *35* (2), 141–167. https://doi.org/10.1016/j.pecs.2008.09.001.

(3) Liu, Y.; Gao, B.; Qiao, Z.; Hu, Y.; Zheng, W.; Zhang, L.; Zhou, Y.; Ji, G.; Yang, G. Gram-Scale Synthesis of Graphene Quantum Dots from Single Carbon Atoms Growth via Energetic Material Deflagration. *Chem. Mater.* **2015**, *27* (12), 4319–4327. https://doi.org/10.1021/acs.chemmater.5b00774.

(4) Zhou, X.; Torabi, M.; Lu, J.; Shen, R.; Zhang, K. Nanostructured Energetic Composites: Synthesis, Ignition/Combustion Modeling, and Applications. *ACS Appl. Mater. Interfaces* **2014**, *6* (5), 3058–3074. https://doi.org/10.1021/am4058138.

(5) Wang, A.; Bok, S.; Thiruvengadathan, R.; Gangopadhyay, K.; McFarland, J. A.; Maschmann, M. R.; Gangopadhyay, S. Reactive Nanoenergetic Graphene Aerogel Synthesized by One-Step Chemical Reduction. *Combustion and Flame* **2018**, *196*, 400–406. https://doi.org/10.1016/j.combustflame.2018.06.034.

(6) Nicollet, A.; Lahiner, G.; Belisario, A.; Souleille, S.; Djafari-Rouhani, M.; Estève, A.; Rossi, C. Investigation of Al/CuO Multilayered Thermite Ignition. *Journal of Applied Physics* **2017**, *121* (3), 034503. https://doi.org/10.1063/1.4974288.

(7) Taton, G.; Lagrange, D.; Conedera, V.; Renaud, L.; Rossi, C. Micro-Chip Initiator Realized by Integrating Al/CuO Multilayer Nanothermite on Polymeric Membrane. *J. Micromech. Microeng.* **2013**, *23* (10), 105009. https://doi.org/10.1088/0960-1317/23/10/105009.

(8) Guo, W.; Chang, S.; Cao, J.; Wu, L.; Shen, R.; Ye, Y. Precisely Controlled Reactive Multilayer Films with Excellent Energy Release Property for Laser-Induced Ignition. *Nanoscale Res Lett* **2019**, *14* (1), 301. https://doi.org/10.1186/s11671-019-3124-6.

(9) Zhang, D.; Pei, R.; Peng, X.; Xiang, Q.; Wang, X. Environment-Friendly Formation of High Energetic Nano-Al/Fe2O3 Bilayer by Aqueous Electrophoretic Deposition. *Propellants, Explosives, Pyrotechnics n/a* (n/a). https://doi.org/10.1002/prep.201900025.

(10) Xu, J.; Tai, Y.; Shen, Y.; Dai, J.; Xu, W.; Ye, Y.; Shen, R.; Hu, Y. Characteristics of Energetic Semiconductor Bridge Initiator Based on Different Stoichiometric Ratios of Al/MoO3 Reactive Multilayer Films under Capacitor Discharge Conditions. *Sensors and Actuators A: Physical* **2019**, *296*, 241–248. https://doi.org/10.1016/j.sna.2019.07.015.

(11) Martirosyan, K. S.; Wang, L.; Vicent, A.; Luss, D. Nanoenergetic Gas-Generators: Design and Performance. *Prop., Explos., Pyrotech.* **2009**, NA-NA. https://doi.org/10.1002/prep.200800059.

(12) Wu, T.; Wang, X.; Zavalij, P. Y.; DeLisio, J. B.; Wang, H.; Zachariah, M. R. Performance of Iodine Oxides/Iodic Acids as Oxidizers in Thermite Systems. *Combustion and Flame* **2018**, *191*, 335–342. https://doi.org/10.1016/j.combustflame.2018.01.017.

(13) Jacob, R. J.; Hill, K. J.; Yang, Y.; Pantoya, M. L.; Zachariah, M. R. Pre-Stressing Aluminum Nanoparticles as a Strategy to Enhance Reactivity of Nanothermite Composites. *Combustion and Flame* **2019**, *205*, 33–40. https://doi.org/10.1016/j.combustflame.2019.03.024.

(14) Wang, H.; Rehwoldt, M.; Kline, D. J.; Wu, T.; Wang, P.; Zachariah, M. R. Comparison Study of the Ignition and Combustion Characteristics of Directly-Written Al/PVDF, Al/Viton and Al/THV Composites. *Combustion and Flame* **2019**, *201*, 181–186. https://doi.org/10.1016/j.combustflame.2018.12.031.

(15) Hastings, D. L.; Schoenitz, M.; Dreizin, E. L. High Density Reactive Composite Powders. *Journal of Alloys and Compounds* **2018**, *735*, 1863–1870. https://doi.org/10.1016/j.jallcom.2017.11.345.

(16) Qin, L.; Gong, T.; Hao, H.; Wang, K.; Feng, H. Core–Shell-Structured Nanothermites Synthesized by Atomic Layer Deposition. *J Nanopart Res* **2013**, *15* (12), 2150. https://doi.org/10.1007/s11051-013-2150-z.

(17) Levitas, V. I.; McCollum, J.; Pantoya, M. Pre-Stressing Micron-Scale Aluminum Core-Shell Particles to Improve Reactivity. *Scientific Reports* **2015**, *5*, 7879. https://doi.org/10.1038/srep07879.

(18) Petrantoni, M.; Rossi, C.; Salvagnac, L.; Conédéra, V.; Estève, A.; Tenailleau, C.; Alphonse, P.; Chabal, Y. J. Multilayered Al/CuO Thermite Formation by Reactive Magnetron Sputtering: Nano versus Micro. *Journal of Applied Physics* **2010**, *108*.

(19) Adams, D. P. Reactive Multilayers Fabricated by Vapor Deposition: A Critical Review. *Thin Solid Films* **2015**, *576*, 98–128. https://doi.org/10.1016/j.tsf.2014.09.042.

(20) Yarrington, C. D.; Abere, M. J.; Adams, D. P.; Hobbs, M. L. Reactive Nanolaminate Pulsed-Laser Ignition Mechanism: Modeling and Experimental Evidence of Diffusion Limited Reactions. *Journal of Applied Physics* **2017**, *121* (13), 134301. https://doi.org/10.1063/1.4979578.

(21) Blobaum, K. J.; Wagner, A. J.; Plitzko, J. M.; Van Heerden, D.; Fairbrother, D. H.; Weihs, T. P. Investigating the Reaction Path and Growth Kinetics in CuOx/Al Multilayer Foils. *Journal of Applied Physics* **2003**, *94* (5), 2923–2929. https://doi.org/10.1063/1.1598297.

(22) Xu, J.; Shen, Y.; Wang, C.; Dai, J.; Tai, Y.; Ye, Y.; Shen, R.; Wang, H.; Zachariah, M. R. Controlling the Energetic Characteristics of Micro Energy Storage Device by in Situ Deposition Al/MoO3 Nanolaminates with Varying Internal Structure. *Chemical Engineering Journal* **2019**, *373*, 345–354. https://doi.org/10.1016/j.cej.2019.04.205.

(23) Zhu, P.; Shen, R.; Ye, Y.; Fu, S.; Li, D. Characterization of Al/CuO Nanoenergetic Multilayer Films Integrated with Semiconductor Bridge for Initiator Applications. *Journal of Applied Physics* **2013**, *113* (18), 184505. https://doi.org/10.1063/1.4804315.

(24) Glavier, L.; Nicollet, A.; Jouot, F.; Martin, B.; Barberon, J.; Renaud, L.; Rossi, C. Nanothermite/RDX-Based Miniature Device for Impact Ignition of High Explosives. *Propellants, Explosives, Pyrotechnics* **2017**, *42* (3), 308–317. https://doi.org/10.1002/prep.201600154.

(25) Kinsey, A. H.; Slusarski, K.; Woll, K.; Gibbins, D.; Weihs, T. P. Effect of Dilution on Reaction Properties and Bonds Formed Using Mechanically Processed Dilute Thermite Foils. *J Mater Sci* **2016**, *51* (12), 5738–5749. https://doi.org/10.1007/s10853-016-9876-9.

(26) Rossi, C. Engineering of Al/CuO Reactive Multilayer Thin Films for Tunable Initiation and Actuation. *Prop., Explos., Pyrotech.* **2019**, *44* (1), 94–108. https://doi.org/10.1002/prep.201800045.

(27) Manesh, N. A.; Basu, S.; Kumar, R. Experimental Flame Speed in Multi-Layered Nano-Energetic Materials. *Combustion and Flame* **2010**, *157* (3), 476–480. https://doi.org/10.1016/j.combustflame.2009.07.011.

(28) Lahiner, G.; Nicollet, A.; Zapata, J.; Marín, L.; Richard, N.; Rouhani, M. D.; Rossi, C.; Estève, A. A Diffusion–Reaction Scheme for Modeling Ignition and Self-Propagating Reactions in Al/CuO Multilayered Thin Films. *Journal of Applied Physics* **2017**, *122* (15), 155105. https://doi.org/10.1063/1.5000312.

(29) Bahrami, M.; Taton, G.; Conédéra, V.; Salvagnac, L.; Tenailleau, C.; Alphonse, P.; Rossi, C. Magnetron Sputtered Al-CuO Nanolaminates: Effect of Stoichiometry and Layers Thickness on Energy Release and Burning Rate. *Propellants, Explosives, Pyrotechnics* **2014**, *39* (3), 365–373. https://doi.org/10.1002/prep.201300080.

(30) Mily, E. J.; Oni, A.; Lebeau, J. M.; Liu, Y.; Brown-Shaklee, H. J.; Ihlefeld, J. F.; Maria, J.-P. The Role of Terminal Oxide Structure and Properties in Nanothermite Reactions. *THIN SOLID FILMS* **2014**, *562*, 405–410. https://doi.org/10.1016/j.tsf.2014.05.005.
(31) Marín, L.; Nanayakkara, C. E.; Veyan, J.-F.; Warot-Fonrose, B.; Joulie, S.; Estève, A.; Tenailleau, C.; Chabal, Y. J.; Rossi, C. Enhancing the Reactivity of Al/CuO Nanolaminates by Cu Incorporation at the Interfaces. *ACS Appl. Mater. Interfaces* **2015**, *7* (22), 11713–11718. https://doi.org/10.1021/acsami.5b02653.
(32) Kinsey, A. H.; Slusarski, K.; Sosa, S.; Weihs, T. P. Gas Suppression via Copper Interlayers in Magnetron Sputtered Al–Cu $_2$ O Multilayers. *ACS Appl. Mater. Interfaces* **2017**, *9* (26), 22026–22036. https://doi.org/10.1021/acsami.7b03071.
(33) Marín, L.; Gao, Y.; Vallet, M.; Abdallah, I.; Warot-Fonrose, B.; Tenailleau, C.; Lucero, A. T.; Kim, J.; Esteve, A.; Chabal, Y. J.; Rossi, C. Performance Enhancement via Incorporation of ZnO Nanolayers in Energetic Al/CuO Multilayers. *Langmuir* **2017**, *33* (41), 11086–11093. https://doi.org/10.1021/acs.langmuir.7b02964.
(34) Zapata, J.; Nicollet, A.; Julien, B.; Lahiner, G.; Esteve, A.; Rossi, C. Self-Propagating Combustion of Sputter-Deposited Al/CuO Nanolaminates. *Combustion and Flame* **2019**, *205*, 389–396. https://doi.org/10.1016/j.combustflame.2019.04.031.
(35) Cure, J.; Assi, H.; Cocq, K.; Marìn, L.; Fajerwerg, K.; Fau, P.; Bêche, E.; Chabal, Y. J.; Estève, A.; Rossi, C. Controlled Growth and Grafting of High-Density Au Nanoparticles on Zinc Oxide Thin Films by Photo-Deposition. *Langmuir* **2018**, *34* (5), 1932–1940. https://doi.org/10.1021/acs.langmuir.7b04105.
(36) Stoney, G. G.; Parsons, C. A. The Tension of Metallic Films Deposited by Electrolysis. *Proceedings of the Royal Society of London. Series A, Containing Papers of a Mathematical and Physical Character* **1909**, *82* (553), 172–175. https://doi.org/10.1098/rspa.1909.0021.
(37) DeLisio, J. B.; Yi, F.; LaVan, D. A.; Zachariah, M. R. High Heating Rate Reaction Dynamics of Al/CuO Nanolaminates by Nanocalorimetry-Coupled Time-of-Flight Mass Spectrometry. *J. Phys. Chem. C* **2017**, *121* (5), 2771–2777. https://doi.org/10.1021/acs.jpcc.6b11114.
(38) Abdallah, I.; Zapata, J.; Lahiner, G.; Warot-Fonrose, B.; Cure, J.; Chabal, Y.; Esteve, A.; Rossi, C. Structure and Chemical Characterization at the Atomic Level of Reactions in Al/CuO Multilayers. *ACS Appl. Energy Mater.* **2018**, *1* (4), 1762–1770. https://doi.org/10.1021/acsaem.8b00296.
(39) Lahiner, G.; Zappata, J.; Cure, J.; Richard, N.; Djafari-Rouhani, M.; Estève, A.; Rossi, C. A Redox Reaction Model for Self-Heating and Aging Prediction of Al/CuO Multilayers. *Combustion Theory and Modelling* **2019**, *23* (4), 700–715. https://doi.org/10.1080/13647830.2019.1584336.
(40) Dong, X.; Fang, X.; Feng, X.; Hwang, K.-C. Diffusion and Stress Coupling Effect during Oxidation at High Temperature. *Journal of the American Ceramic Society* **2013**, *96* (1), 44–46. https://doi.org/10.1111/jace.12105.
(41) Wang, Y.; Lany, S.; Ghanbaja, J.; Fagot-Revurat, Y.; Chen, Y. P.; Soldera, F.; Horwat, D.; Mücklich, F.; Pierson, J. F. Electronic Structures of Cu2O, Cu4O3, and CuO: A Joint Experimental and Theoretical Study. *Phys. Rev. B* **2016**, *94* (24), 245418. https://doi.org/10.1103/PhysRevB.94.245418.
(42) Leapman, R. D.; Grunes, L. A.; Fejes, P. L. Study of the ${L}_{23}$ Edges in the $3d$ Transition Metals and Their Oxides by Electron-Energy-Loss Spectroscopy with

Comparisons to Theory. *Phys. Rev. B* **1982**, *26* (2), 614–635. https://doi.org/10.1103/PhysRevB.26.614.
(43) Jiang, N.; Spence, J. C. H. Interpretation of Oxygen K Pre-Edge Peak in Complex Oxides. *Ultramicroscopy* **2006**, *106* (3), 215–219. https://doi.org/10.1016/j.ultramic.2005.07.004.